High-efficiency Mid-infrared Wavelength Conversion in Silicon Waveguides

T. Chen¹, M. Huang¹, S. Sun¹, C. Stirling¹, C. Mitchell¹, M. Nedeljkovic¹, G. Z. Mashanovich¹, and A. C. Peacock^{1*}
¹Optoelectronics Research Centre, University of Southampton, Southampton SO17 1BJ, United Kingdom
*Correspondence E-mail: acp@orc.soton.ac.uk

Abstract—High-efficiency wavelength conversion into the 2 µm region has been achieved through Raman enhanced fourwave mixing in a planar silicon waveguide. By aligning the FWM phase-matching conditions with the Raman gain bandwidth, a wavelength conversion efficiency of -25 dB was achieved with a continuous-wave pump power of only ~45 mW. The maximum Raman enhancement in this hybrid wavelength conversion process is ~7 dB. Simulations show that by further optimizing the planar waveguide dispersion profile, the wavelength conversion efficiency could be increased to ~-11 dB using a standard continuous-wave pump source.

I, Introduction

Silicon photonic platforms that operate in the wavelength range covering 2-3 µm have been generating increased interest due to their potential use in broadband communications [1], optical imaging [2], and sensing [3]. Although there applications are integrated semiconductor-based laser systems available in this region, they are typically restricted to operating in discrete wavelength bands that are fixed by the choice of gain medium [4]. The ability to make use of the excellent nonlinear transmission properties of silicon waveguides to tune and extend the wavelength coverage of the light sources is thus highly advantageous for the development of practical and compact systems [5].

Of the various nonlinear processes, four-wave mixing (FWM) has been the most extensively explored for the generation and manipulation of new wavelengths extending beyond 2 µm [6]. However, in order to achieve high conversion efficiencies (CEs), pulsed pump sources are often used due to their high peak powers, but also to reduce the build-up of free carriers that can result in significant absorption in silicon systems [7]. From a practical perspective, continuous-wave (CW) pumping is more desirable as the lasers are usually more stable, lower cost, and more suited for direct integration [8]. Popular approaches to increasing the efficiency of CW pumped systems include making use of resonator geometries to increase the interaction length [9] or incorporating PIN junctions to reduce the free carrier losses [10]. An alternative method that has been demonstrated recently in the telecom band is to couple the FWM process with the strong resonant Raman gain associated with the crystalline silicon core [11]. The advantage of this approach is that standard waveguide structures can be employed, simplifying the geometry, whilst the combination of FWM and Raman still allows for

tunability of the system when combined with tunable thulium-doped fiber lasers operating around 2 µm.

In this paper we demonstrate strong Raman enhancement of FWM wavelength conversion in silicon waveguides designed for operation in the 2-3 μm region. A maximum conversion efficiency of around -25 dB has been achieved with a CW pump power of only ~45 mW, significantly more efficient than previous FWM results in this regime [12, 13]. Numerical modelling of the nonlinear interactions indicates an enhancement in the FWM CE due to coupling with the strong Raman effect of ~7 dB. Moreover, the modelling predicts that the conversion efficiency could be increased to ~-11 dB with an appropriate dispersion profile and realistic pump powers of ~200 mW. These promising results highlight the advantage of exploiting Raman enhanced FWM processes to improve the efficiency and practicality of planar integrated silicon systems in the 2-3 μm region.

II, Concept and Setup

A. Theory of Raman Enhanced FWM

Raman enhanced FWM involves three nonlinear effects: (1) degenerate FWM, (2) stimulated Raman scattering (SRS), and (3) inverse Raman scattering (IRS) [14]. The process is similar to coherent anti-Stokes Raman scattering (CARS), which has been investigated quite extensively in silicon waveguides [15], but here the signal wavelength is aligned to convert anti-Stokes photons to Stokes photons in order to take advantage of the higher Raman gain [11, 16]. Figure 1(a) shows the energy level diagrams for these three processes. Degenerate FWM is a nonlinear effect where two pump photons with frequency ω_p are used to generate an idler photon (ω_i) and a signal photon (ω_s) , which must obey conservation of energy: $2\omega_p = \omega_i + \omega_s$. In SRS, the pump photon (ω_n) will interact with the nonlinear medium, resulting in a vibration and a red-shift Stokes photon (ω_{st}), with a Raman shift determined by the phonon frequency $(\Delta\omega_{\nu})$ such that: $\omega_{p} = \omega_{st} + \Delta\omega_{\nu}$. In IRS, the pump beam (ω_p) acts as the seed beam, which will be enhanced by the applied anti-Stokes beam as: $\omega_p = \omega_{as} - \Delta \omega_{\nu}$. If the FWM process is selected to overlap with Raman scattering such that $\omega_s = \omega_{as}$ and $\omega_i = \omega_{st}$ for the given pump wavelength, then the wavelength conversion can be significantly enhanced by the combination of the processes in Figure 1(a), starting with process (1) through to process (3).

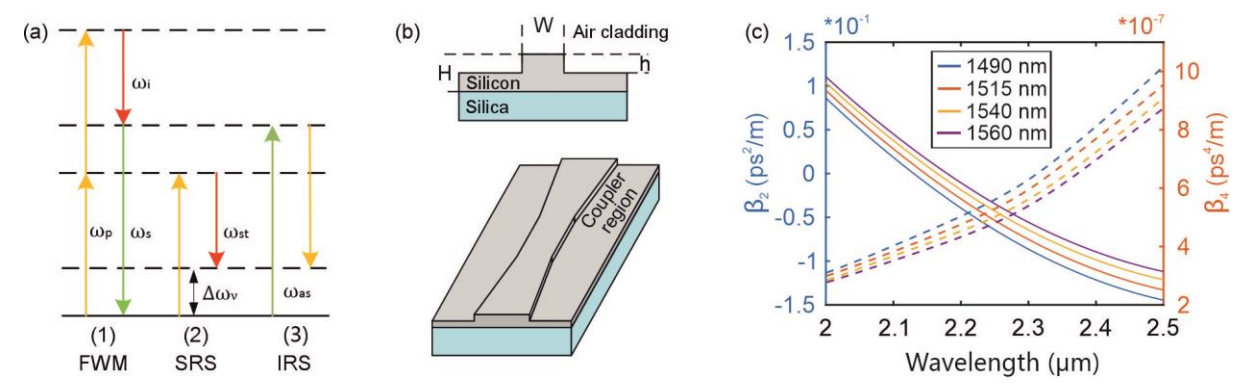


Figure 1 (a) Energy level diagrams for (1) FWM, (2) SRS, and (3) IRS. (b) Schematics of the cross-section and the longitudinal profile of the planar silicon rib waveguides. (c) Calculated group velocity dispersion (GVD, solid lines) and fourth order dispersion (FOD, dashed lines) as a function of wavelength for the rib waveguides with widths as labelled in the legend.

B. Waveguide Design

To take advantage of the Raman enhancement, it is important to keep the intrinsic FWM CE high enough to act as the seed for SRS. Thus, precise dispersion engineering of the silicon waveguide is required to achieve phase-matching for the pump wavelength. In our work, we make use of rib waveguide structures as they can be fabricated to have low transmission losses in the 2-3 µm region [17]. The crosssection of the rib design is shown in Figure 1(b), which includes three key parameters: rib width (W), etch depth (h), and rib height (H). Two waveguide designs were considered, both with a zero-dispersion wavelength (ZDW) near the pump wavelength (~2.17 µm), but with slightly different widths so that the role of phase-matching can be investigated [16]. The silicon rib waveguides used in this experiment were fabricated with electron-beam lithography followed by a dry etching process, which gives very precise dimensional control [18]. To facilitate coupling into the optimized rib section, two tapered regions were added to each end to increase the waveguide widths at the facets, as shown in Figure 1(b). However, these tapered couplers were kept sufficiently short so that they did not contribute to the nonlinear propagation. Since the pump wavelength is close to the ZDW, terms up to fourth-order dispersion were included for the calculations. The group velocity dispersion (GVD) and fourth-order dispersion (FOD) of rib waveguides with different widths are calculated using the refractive indices of silicon [19] and silica [20] from the literature, and shown in Fig. 1(c).

Table 1 Design parameters for the silicon rib waveguides for Raman enhanced FWM.

Label	WG1	WG2
Input coupler width (μm)	15	15
Rib width (µm)	1.515	1.490

Output coupler width (µm)	15	15
Rib height (nm)	500	500
Slab height (nm)	250	250
Waveguide length (cm)	2	2
Calculated β_2 (ps ² /m)	-0.013	-0.023
Propagation loss (dB/cm)	~2.5	~2.5

The parameters for the two waveguides are given in Table 1. WG1 has a GVD term (β_2 =-0.013 ps²/m at 2.17 µm) closer to zero, which suggests it should have a better phasematching condition for FWM. Considering the total insertion losses (~20 dB) of these two waveguides, and previous determination of the coupling losses through cut-back measurements, the propagation losses for both waveguides were estimated to be ~2.5 dB/cm. Further confirmation of the loss values was obtained via simulations to fit the experimental results of Raman enhanced FWM. We attribute the higher propagation losses of our waveguides, when compared to state-of-the-art foundry SOI platforms, to slightly higher sidewall roughness values. Thus, the waveguide losses could be improved in future work through further optimization of the etching recipes or via adding a thin capping layer via atomic layer deposition to smooth the surfaces [21].

C. Setup

The experimental setup is shown in Figure 2. Due to the limited access to tunable sources around 1900 nm, we used a fixed wavelength CW laser (LFLTM) positioned at 1950 nm as the signal. A tunable CW pump laser (Cr+2: ZnS/Se IPG Photonics) covering the range 2165 nm to 2172 nm was then employed to ensure the generated idler wave could be tuned through the Raman gain bandwidth (2440-2450 nm). A beam splitter (BS) (9:1) was used to combine the pump and signal

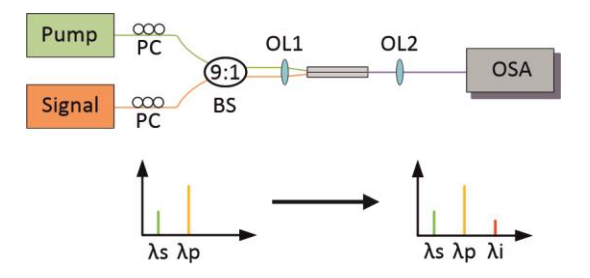


Figure 2 Experimental setup for Raman enhanced FWM. OL1 & OL2: objective lenses; BS: beam splitter; OSA: optical spectrum analyzer; PC: polarization controller.

laser, before coupling into and out of the silicon waveguides by using two aspherical objective lenses (OL) (C093TME-D). The output beam was collected using a mid-infrared fiber (Thorlabs, M43L01, transmission window of 400 nm – 2400 nm) to ensure a high coupling efficiency. The collected light was then sent to a mid-infrared OSA (YOKOGAWA, AQ6376) to measure the FWM spectra. Two polarizers were used for the pump and signal input beams to ensure the light propagated within the TE1 mode in the waveguides.

III、 Result and Discussion

A representative transmission spectrum as measured from the output of WG1 is shown in Fig. 3(a). Using the measured coupling losses, the coupled-in power for the signal and pump lasers were estimated to be $\sim 90~\mu W$ and $\sim 45~mW$, respectively. When the idler is tuned across the Raman gain bandwidth, the CE ($P_{idler}^{out}/P_{signal}^{in}$) of WG1 and WG2 varies as shown in Fig. 3(b). With the generated idler wavelength aligned to the central wavelength of Raman gain peak, the CE in WG1 increased from $\sim -32~dB$ to $\sim -25~dB$, indicating an enhancement of $\sim 7~dB$ due to the coupling of the nonlinear processes. In WG2, the enhancement is less pronounced, but there is still an increase from $\sim -38~dB$ to $\sim -34~dB$ We attribute the reduction in the CE for WG2 to the larger GVD of the waveguide and the less optimum FWM.

To investigate the coupling of the FWM and Raman processes in more detail, nonlinear propagation in the waveguides was modelled via the generalized nonlinear Schrödinger equation (GNLSE) [14]:

$$\begin{array}{l} \frac{\partial A}{\partial z} + \frac{\alpha}{2}A - i\sum_{n=1}^{\infty}\frac{i^{n}\beta_{n}}{n!}\frac{\partial^{n}A}{\partial t^{n}} - \frac{\sigma}{2}(1+i\mu)N_{c}A = \\ i\left(\gamma(\omega_{0}) + i\gamma_{1}\frac{\partial}{\partial t}\right)\left(A\int_{0}^{\infty}R(t')|A(z,t-t')|^{2}\ dt'\right). \end{array} \tag{1}$$

Here A is the amplitude of pump laser, which we approximate as a quasi-CW beam. α is the linear propagation loss; β_n is the nth order dispersive term; $\gamma = \omega_0 n_2/cA_{eff} + i \beta_{TPA}/2A_{eff}$ is the nonlinear parameter, where n_2 is the nonlinear refractive index and A_{eff} is the effective mode area; $\gamma_1 = (d\gamma/d\omega)_{\omega=\omega_0}$; σ is the free carrier loss and μ is the free carrier dispersion. N_c is the free carrier density which is governed by the following equation:

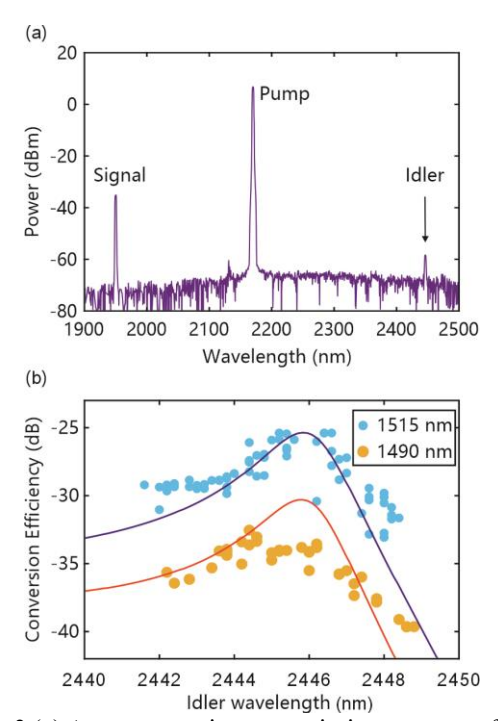


Figure 3 (a) A representative transmission spectrum from the output of WG1. (b) Conversion efficiency as a function of idler wavelength with the signal at 1950 nm and the pump wavelength tuned from 2165 nm to 2172 nm.

$$\frac{\partial N_c(t)}{\partial t} = \frac{\beta_{TPA}}{2\hbar\omega_0} \frac{|E(t)|^4}{A_{eff}^2} - \frac{N_c(t)}{\tau},\tag{2}$$

where β_{TPA} is the two-photon absorption coefficient and τ is the free-carrier lifetime. The nonlinear response function R(t) is given by:

$$R(t) = (1 - f_R)\delta(t) + f_R h_R(t),$$
 (3)

where $f_R = g_R \Gamma_R/(n_2 k_0 \Omega_R)$ represents the fractional contribution of the delayed Raman response to the nonlinear polarization in which g_R is the Raman gain, Γ_R/π is the gain bandwidth, $\Omega_R/2\pi$ is the peak gain frequency shift. The Raman response function for silicon is given by: $h_R(t) = (\tau_1^{-2} + \tau_2^{-2})\tau_1 \exp(-t/\tau_2)\sin(t/\tau_1)$, in which τ_1 and τ_2 are the damping times of the Raman vibrations.

For the GNLSE simulations, the wavelength dependent β_n , A_{eff} , n_2 and β_{TPA} values were estimated using the methods described in Ref. [14]. The results of the simulations are plotted in Figure 3(b) using the experimental input power of ~45 mW. The modelled curves are in good agreement with the experimental data, particularly for WG1. The slight disagreement for WG2 is most likely due to power fluctuations during the measurements. Nevertheless, these simulation results show that, regardless of the phasematching, coupling between the FWM and Raman processes can result in a significant enhancement of the CE. Moreover, the CE of Raman enhanced FWM can be increased significantly through increasing the pump power. Figure 4(a) shows the measured and simulated Raman enhanced CE for

WG1 and WG2 as a function of coupled-in pump power. Clearly, the maximum pump power used in these experiments of ~45 mW is still very low. However, the results indicate that by increasing the pump power to ~150 mW, which is readily available with many CW sources, the CE could reach ~-15 dB in WG1.

Traditionally, efficient FWM in silicon waveguides in the 2 μ m wavelength range has required high light intensities. Despite this, the previously achieved CEs are still relatively low. For example, Lau *et al.* reported a CE of approximately -32 dB with a pump intensity on the order of 1×10^{11} W·m⁻² [13], which is one order of magnitude higher than that employed in our work. Based on the simulated CE values, which exhibit excellent agreement with experimental data, it can be estimated that an enhanced CE of -22 dB could be achieved by exploiting Raman enhanced FWM with the same pump intensity as in Ref. [13], as shown by the grey point in Figure 4(a).

Finally, we investigate the role of the dispersion profile on the maximum possible CE. Additional simulations of different waveguide widths reveal that further improvement of the CE could be obtained by optimizing the dispersion profile of the waveguides to expand the FWM phasematching bandwidth. Figure 4(b) shows the simulated CE for WG1 and WG2, as well as two slightly wider waveguide widths of W=1540 nm and 1560 nm, calculated for pumping with a CW power of 200 mW. From the inset we see that the maximum achievable CE peaks for the optimum waveguide width of 1540 nm, and then decreases as the ridge width increases further. Although there is not a dramatic change in the maximum Raman enhanced FWM peak for the four waveguides, the optimized width does offer a small increase in the CE of ~-11 dB compared to the predicted maximum of -12 dB for WG1, thanks to the slightly higher FWM baseline. However, the Raman enhancement remains significant (>14 dB) for all four widths, indicating that the process is robust against fabrication tolerances in the waveguide designs. Moreover, further simulations have also been conducted to investigate the tolerance of the Raman enhanced FWM when tuning the pump from the optimized value for a given waveguide design. The results have shown that although there is some decrease in the maximum CE, as expected due to the reduction of the FWM efficiency, coupling to the Raman term helps to partially compensate for this, so that the overall CE for the hybrid system is higher than for FWM alone. Interestingly, when the optimum width of 1540 nm is selected in Fig. 4(b), the very flat and broad FWM gain bandwidth offers the potential to extend the idler light to longer wavelengths through cascaded Raman enhanced FWM processes [22]. Thus, Raman enhanced FWM schemes offer great potential for high efficiency and tunable sources of mid-infrared light.

IV, Conclusion

In conclusion, we have shown that by coupling the Raman and FWM nonlinear processes in a silicon waveguide, it is

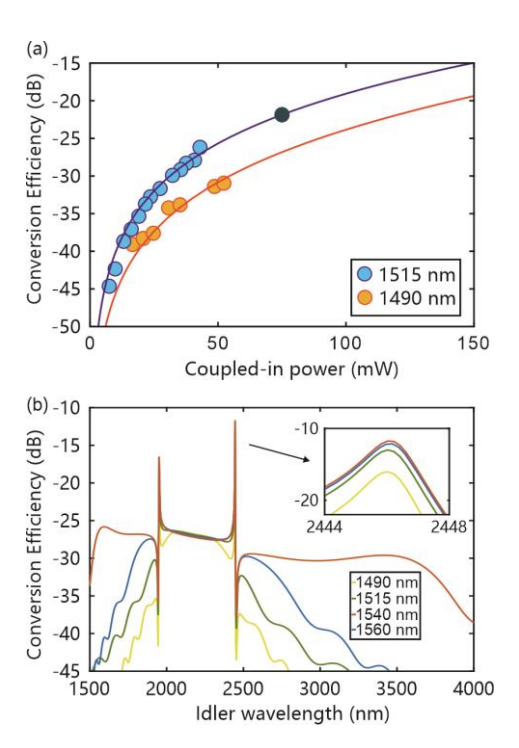


Figure 4 (a) Conversion efficiency as a function of pump power for WG1 & WG2. Grey dot is the estimated Raman enhanced CE using the intensity from Ref. 13 for comparison. (b) Simulated CE for Raman enhanced FWM for waveguides with different widths, as labelled in the legend, when pumped with a coupled in power of 200 mW.

possible to significantly enhance the wavelength conversion efficiency in the mid-infrared regime, where pump powers are often lower than their telecom band equivalents. Moreover, the process can make use of straight waveguides and so does not rely on the fabrication of more complex ring resonators or PIN structures to compensate for losses associated with high power pumps. Our experiments indicate that the peak conversion efficiency is influenced by the phase-matching conditions of the FWM process, with the highest CE obtained when the waveguide is designed to have a broad, flat FWM bandwidth. A maximum enhancement of ~7 dB was obtained for a waveguide with the smallest group velocity dispersion parameter, with an overall CE of ~-25 dB for a modest pump power of ~45 mW. Further adjustment of the waveguide design and pump power could yield higher FWM conversion efficiencies, especially compared with the previous FWM results obtained without Raman. These findings demonstrate the versatility and effectiveness of this method to boost the FWM conversion efficiency in the traditional planar silicon waveguide system.

Acknowledgments

We would like to acknowledge the support from the following funding bodies: Engineering and Physical Sciences Research Council (EPSRC, Grant Nos. EP/Y008499/1 and EP/P000940/1).

Data availability

The data that support the findings of this study are openly available in the University of Southampton at https://doi.org/10.5258/SOTON/D3686, reference number [23].

Reference

- [1] S. Zheng et al., "Silicon-based four-mode division multiplexing for chip-scale optical data transmission in the 2 μ m waveband," Photonics Research, 7(9), 1030 (2019).
- [2] J. S. Dam, P. Tidemand-Lichtenberg, and C. Pedersen, "Room-temperature mid-infrared single-photon spectral imaging," *Nature Photonics*, 6(11), 788 (2012).
- [3] A. G. Griffith *et al.*, "Silicon-chip mid-infrared frequency comb generation," *Nature Communications*, 6(1), 6299 (2015).
- [4] E. Tournie and A. N. Baranov, "Mid-infrared semiconductor lasers: a review," *Semiconductors and Semimetals*, 86, 183 (2012).
- [5] I. Alamgir, F. St-Hilaire, and M. Rochette, "All-fiber nonlinear optical wavelength conversion system from the C-band to the mid-infrared," *Optics Letters*, 45(4), 857 (2020).
- [6] M. A. Foster, A. C. Turner, J. E. Sharping, B. S. Schmidt, M. Lipson, and A. L. Gaeta, "Broad-band optical parametric gain on a silicon photonic chip," *Nature*, 441(7096), 960 (2006).
- [7] F. De Leonardis and V. M. Passaro, "Efficient wavelength conversion in optimized SOI waveguides via pulsed four-wave mixing," *Journal of Lightwave Technology*, 29(23), 3523 (2011).
- [8] H. Rong, Y.-H. Kuo, A. Liu, M. Paniccia, and O. Cohen, "High efficiency wavelength conversion of 10 Gb/s data in silicon waveguides," *Optics Express*, 14(3), 1182 (2006).
- [9] J. R. Ong et al., "Low-power continuous-wave four-wave mixing in silicon coupled-resonator optical waveguides," Optics Letters, 36(15), 2964 (2011).
- [10] A. Gajda et al., "Highly efficient CW parametric conversion at 1550 nm in SOI waveguides by reverse biased pin junction," Optics Express, 20(12), 13100 (2012).
- [11] T. Sylvestre, H. Maillotte, E. Lantz, and P. Tchofo Dinda, "Raman-assisted parametric frequency conversion in a normally dispersive single-mode fiber," *Optics Letters*, 24(22), 1561 (1999).
- [12] S. Zlatanovic *et al.*, "Mid-infrared wavelength conversion in silicon waveguides using ultracompact telecom-band-derived pump source," *Nature Photonics*, 4(8), 561 (2010).
- [13] R. K. Lau et al., "Continuous-wave mid-infrared frequency conversion in silicon nanowaveguides," Optics Letters, 36(7), 1263 (2011).
- [14] S. Sun *et al.*, "Raman enhanced four-wave mixing in silicon core fibers," *Optics Letters*, 47(7), 1626 (2022).
- [15] N. Vermeulen, C. Debaes, and H. Thienpont, "Coherent anti-Stokes Raman scattering in Raman lasers and Raman wavelength converters," *Laser & Photonics Reviews*, 4(5), 656 (2010).
- [16] S. Sun, G. Z. Mashanovich, and A. C. Peacock, "Design of integrated silicon waveguides for Raman-enhanced four-wave mixing in the telecom band," *Optics Express*, 32(6), 8715 (2024).
- [17] D. E. Hagan and A. P. Knights, "Mechanisms for optical loss in SOI waveguides for mid-infrared wavelengths around 2 μm," *Journal of Optics*, 19(2), 025801 (2016).
- [18] G. Z. Mashanovich et al., "Silicon photonic waveguides and devices for near-and mid-IR applications," IEEE Journal of Selected Topics in Quantum Electronics, 21(4), 407 (2014).

- [19] H. Li, "Refractive index of silicon and germanium and its wavelength and temperature derivatives," *Journal of Physical* and Chemical Reference Data, 9(3), 561 (1980).
- [20] R. Kitamura, L. Pilon, and M. Jonasz, "Optical constants of silica glass from extreme ultraviolet to far infrared at near room temperature," *Applied Optics*, 46(33), 8118 (2007).
- [21] T. Alasaarela et al., "Reduced propagation loss in silicon strip and slot waveguides coated by atomic layer deposition," Optics Express, 19(12), 11529 (2011).
- [22] M. Huang *et al.*, "Raman amplification at 2.2 μm in silicon core fibers with prospects for extended mid-infrared source generation," *Light: Science & Applications*, 12(1), 209 (2023).
- [23] M. Huang et al., "Dataset in support of the paper 'High-efficiency Mid-infrared Wavelength Conversion in Silicon waveguides," in EPrints (University of Southampton, 2025).